

Angle-Resolved Auger Spectroscopy as a Sensitive Access to Vibronic Coupling

A. Knie,^{1,*} M. Patanen,^{2,†} A. Hans,¹ I. D. Petrov,^{3,4} J. D. Bozek,² A. Ehresmann,¹ and Ph. V. Demekhin^{1,4,‡}

¹*Institut für Physik und CINSaT, Universität Kassel, Heinrich-Plett-Straße 40, 34132 Kassel, Germany*

²*Synchrotron SOLEIL, L'Orme des Merisiers, Saint-Aubin, BP 48, 91192 Gif-sur Yvette Cedex, France*

³*Rostov State Transport University, Narodnogo Opolcheniya Square 2, 344038 Rostov-on-Don, Russia*

⁴*Research Institute of Physics, Southern Federal University, Stachki Avenue 194, 344090 Rostov-on-Don, Russia*

(Received 20 October 2015; published 12 May 2016)

In the angle-averaged excitation and decay spectra of molecules, vibronic coupling may induce the usually weak dipole-forbidden transitions by the excitation intensity borrowing mechanism. The present complementary theoretical and experimental study of the resonant Auger decay of core-to-Rydberg excited CH₄ and Ne demonstrates that vibronic coupling plays a decisive role in the formation of the angle-resolved spectra by additionally involving the decay rate borrowing mechanism. Thereby, we propose that the angle-resolved Auger spectroscopy can in general provide very insightful information on the strength of the vibronic coupling.

DOI: 10.1103/PhysRevLett.116.193002

Coupling between the nuclear and electronic motions beyond the usually successful Born-Oppenheimer approximation is generally referred to as vibronic coupling [1–3]. Jahn-Teller and Renner-Teller effects, as well as ultrafast nonadiabatic dynamics via conical intersections [4–6] are classical examples of vibronic coupling. The significance of vibronic coupling for the spectroscopy of molecules [7,8] and solids [9,10] is already well understood. It is of particular importance for ultrafast radiationless decay and energy transfer processes in large polyatomic and even biologically relevant molecules [11,12]. The role of vibronic coupling in the photoelectron angular distribution [13] and partial decay rate distribution [14] has also been investigated. Here, we show that vibronic coupling has a dramatic effect on the angle-resolved Auger spectra of molecules and can govern angular distributions of emitted electrons.

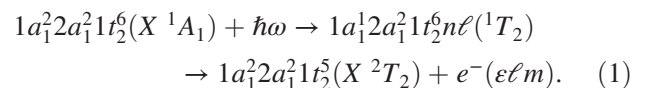
Methane is the prototypical system for studying vibronic coupling effects [15,16]. Its carbon *K*-edge excitation spectrum exhibits a prominent C 1s → *nℓ* Rydberg series [17,18]. The most intense structures in the excitation spectrum are associated with the symmetric stretching (ν_1) mode of the dipole-allowed 1s_{a₁} → *npt*₂ and 1s_{a₁} → *ndt*₂ transitions [19]. The *npt*₂ Rydberg states are split by the Jahn-Teller effect via vibronic coupling through the ν_2 , ν_4 dynamical modes [19] [e.g., overlapping resonances on the high-energy side of the strongest 3*pt*₂($\nu_1 = 0$) resonance]. The weak low-energy side structures in the excitation spectrum are attributed to the dipole-forbidden 1s_{a₁} → 3s_{a₁} electron transition, which becomes vibronically allowed through coupling with the *t*₂(ν_3, ν_4) dynamical modes [17–19]. Those additional resonances are typical examples of the excitation intensity borrowing mechanism [18].

The angular emission distributions are very sensitive to the interplay between the outgoing partial electron continuum waves [20]. Consequently, angular distribution parameters provide very important complementary information on the

competing electron and nuclear dynamics, which may not be accessible in the angle-averaged spectra [21–26]. In this Letter, we utilize this advantage of the angle-resolved Auger electron spectroscopy [27] to study vibronic coupling effects in core-to-Rydberg excited methane. Specifically, we investigate experimentally and theoretically the participator resonant Auger decay populating the ground CH₄⁺(*X* 1*t*₂⁻¹) final ionic state and analyze the angular anisotropy parameters of the emitted electrons.

It will become evident that the *ab initio* electronic structure and nuclear dynamics calculations, which involve the symmetric stretching vibrational mode and the already known excitation intensity borrowing mechanism via vibronic coupling, fail to explain the presently observed angle-resolved spectra of methane. In order to cross-check those theoretical results, we performed an additional angle-resolved study of the corresponding participator resonant Auger decay of the Ne 1s → 3*p* resonance populating the Ne⁺(2*p*⁻¹) ground ionic state, and we obtained excellent agreement between theory and experiment. The probability for resonant Auger processes is proportional to the product of the oscillator strength for resonant excitation and the partial rate for decay into the final continuum state. Each of these ingredients is sensitive to vibronic coupling effects. Therefore, we propose an additional mechanism: the decay rate borrowing via vibronic coupling. Simulations involving this novel mechanism enabled a successful interpretation of the presently measured angle-resolved resonant Auger spectra of CH₄.

The process relevant to the present study of methane can be schematically represented as follows:



At first, linearly polarized synchrotron radiation with the energy of $\hbar\omega \sim 288$ eV excites the C 1s electron into

Rydberg states. In the second step, these excited electrons take part in the Auger decay, which leaves methane in the $X\ 1t_2^{-1}$ ionic state with the binding energy of 14.25 eV [28], and a high-energy electron is emitted. Alternatively, the same final ionic state can be populated via the nonresonant photoionization of the $1t_2$ valence shell. Notwithstanding the high photon energy, this direct ionization channel plays a very important role [29,30].

The present experiments were performed in the Auger-Raman regime [31,32] at the PLEIADES beam line, SOLEIL synchrotron radiation facility. The experimental setup and procedure to determine electron angular distributions are similar to that reported in Refs. [33–35]. For methane, the energy of the synchrotron radiation was varied in steps of 25 meV in the range of 286.7–290.0 eV, and the photon bandwidth of 70 meV was smaller than the natural lifetime width of 94 ± 1 meV of the C $1s$ hole [36]. For neon, the energy range of 865.6–869.0 eV was covered in steps of 100 meV at a photon bandwidth of about 150 meV, which again was smaller than the Ne $1s$ -hole decay width of 270 ± 20 meV [37]. The photon energy was calibrated to data from Refs. [19,37]. The electron spectra were recorded using a VG Scienta R4000 hemispherical analyzer. For the present purposes, it was sufficient to acquire low electron energy resolution spectra for the whole $\text{CH}_4^+(X\ 1t_2^{-1})$ band and for the whole Ne $2p_{1/2,3/2}$ doublet. The spectra were normalized with respect to photon flux, pressure, and acquisition time to ensure a reliable determination of the angular anisotropy parameters.

To describe process (1), we applied the theoretical approach from our previous angle-resolved studies of core-excited molecules [21,22,24,25,38]. Potential energy curves of methane were computed by the multireference configuration interaction method. The core-excited states we treated in the equivalent core “ $Z + 1$ ” approximation. Electronic transition amplitudes were computed by the single center method [39], which was recently extended to polyatomics [40]. Calculations were performed at the equilibrium internuclear geometry of the ground electronic state of CH_4 in the relaxed-core Hartree-Fock approximation. In the calculations, the lifetime vibrational interference [41] and the electronic state interference [42] between direct and resonant amplitudes for the population of the final ionic states were taken into account. The equations for computing transition amplitudes in the vicinity of the core excitation, the total cross section, and the angular distribution parameter of the resonant Auger electrons in polyatomic molecules are reported in Ref. [38].

The photoionization cross section $\sigma_X(\omega)$ for the $\text{CH}_4^+(X\ 1t_2^{-1})$ state and the corresponding angular distribution parameter $\beta_X^e(\omega)$ measured and computed in the present work in the vicinity of the core excitation of methane are collected in Fig. 1. This figure illustrates data for the whole vibrationally unresolved band since vibrational structures of the $\text{CH}_4^+(X\ 1t_2^{-1})$ state strongly overlap [19,43].

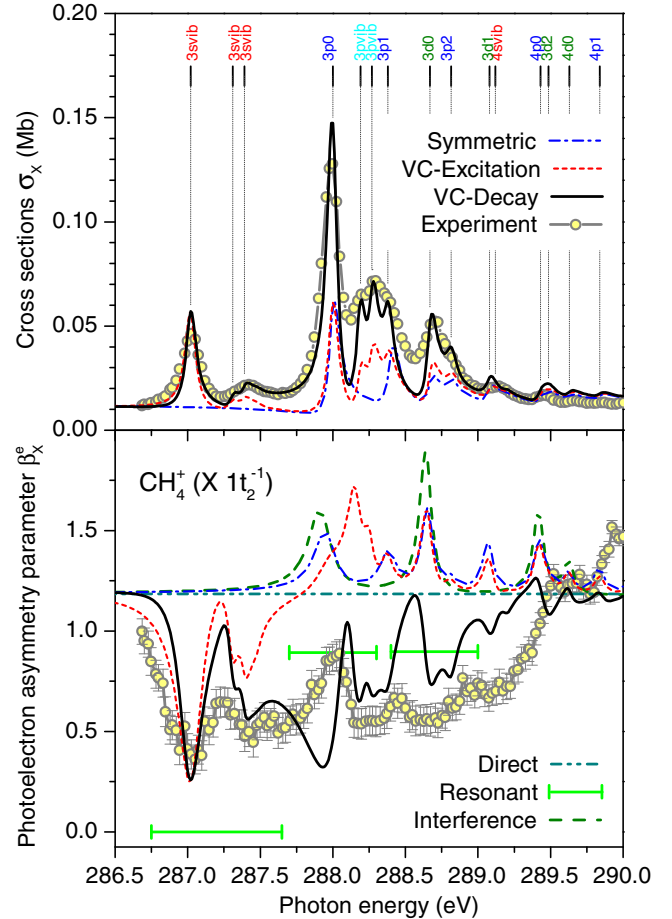


FIG. 1. Photoionization cross section (upper panel) and angular distribution parameter (lower panel) measured (open circles) and computed in different approximations in the vicinity of the C $1s \rightarrow n\ell$ excitations for the participator $\text{CH}_4^+(X\ 1t_2^{-1})$ final ionic state. The experimental cross section is set on absolute scale with the help of the final theoretical result (the black solid curve), whereas no normalization for the asymmetry parameter is required. Calculations performed without including nuclear motion (see the legend in the lower panel) illustrate individual $\beta_X^e(\omega)$ parameters for the direct (cyan dash-dot-dotted line) and resonant (green horizontal bars) ionization channels, and for their interference (the green dashed curve). The $\sigma_X(\omega)$ and $\beta_X^e(\omega)$ computed by including the symmetric stretching mode (the blue dash-dotted curve), as well as through the present simulation of the excitation intensity borrowing via vibronic coupling (VC Excitation, red short-dashed curve) and the decay rate borrowing via vibronic coupling (VC Decay, black solid curve), are also shown (see the upper legend and the text for details). Assignments of the vibronic resonances $n\ell\nu_1$ and $n\ell\nu_{\text{vib}}$ (“vib” stands for ν_2 – ν_4) made according to Refs. [17–19] are indicated at the top.

Calculations were performed in different approximations. We first discuss results obtained by neglecting the nuclear motion and including only electronic transitions. The individual β_X^e parameters obtained separately for the $3s$, $3p$, and $3d$ resonances (Resonant) and for the direct

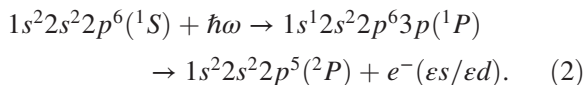
TABLE I. The presently computed properties of the C $1s^{-1}n\ell$ Rydberg electrons of methane ($n\ell = 3s_{a_1}$, $3p_{t_2}$, and $3d_{t_2}$). Listed are the one-electron energy ε , two prevailing contributions from partial momenta $|\langle\ell|\ell\rangle|^2$, the oscillator strength for the excitation $\sigma_{1s}^{n\ell}$, and the partial participator Auger decay rate $\Gamma_X^{n\ell}$.

$n\ell$	ε (eV)	$ \langle\ell \ell\rangle ^2$ (%)	$\sigma_{1s}^{n\ell}$ (kb a.u.)	$\Gamma_X^{n\ell}$ (meV)
$3s$	-3.46	99.7(s)	0.3(f)	0.0
$3p$	-2.48	99.5(p)	0.5(d)	54.2
$3d$	-1.67	1.8(p)	97.7(d)	18.1

transition (Direct) are shown in the lower panel of Fig. 1 by green horizontal bars and a cyan dashed-dot-dotted horizontal line, respectively. Some properties of the Rydberg states computed in the present work are collected in Table I.

The interference between direct and resonant electronic channels introduces a sharp energy dependence of the computed $\beta_X^e(\omega)$ across the position of the electronic resonances [29,30] (Interference, green dashed curve). Only dipole-allowed $3p$, $3d$, $4p$, and $4d$ states, which fall in the considered energy range, are clearly manifested in $\beta_X^e(\omega)$, whereas dipole-forbidden $3s$ and $4s$ states are absent. Far away from the resonances, $\beta_X^e(\omega)$ is determined by the direct ionization channel (cyan dashed-dot-dotted horizontal line) and is calculated to be 1.19. Intuitively, at the positions of the resonances, it is expected to decrease to its purely resonant value of about 0.9. Instead of doing so, $\beta_X^e(\omega)$ rises significantly around each dipole-allowed resonance. However, this interesting computational result is in contradiction to the present measurements. From the lower panel of Fig. 1, it is evident that the experimental $\beta_X^e(\omega)$ exhibits a broad dip across the resonances.

The agreement between theory and experiment does not improve if the symmetric stretching dynamical mode is included in the calculations (the blue dash-dotted curves in the figure). As expected [19], the computed $\sigma_X(\omega)$ and $\beta_X^e(\omega)$ exhibit significantly more resonances since $\nu_1 = 0, 1$, and 2 vibrational levels can now be excited for each electronic state (see the assignment at the top of Fig. 1). Nevertheless, the computed $\beta_X^e(\omega)$ parameter still has a counterintuitive energy dependence of a peak type. Because of this disagreement, we performed a separate theoretical and experimental study of a similar decay in the Ne atom, where nuclear dynamics is naturally absent. We thus have measured and computed $\sigma_{2p}(\omega)$ and $\beta_{2p}^e(\omega)$ for the following process:



In the calculations, we utilized the same computer codes and working equations as with methane.

Figure 2 illustrates the very good agreement between the presently computed (red solid curves) and measured (open circles) angle-resolved participator Auger electron

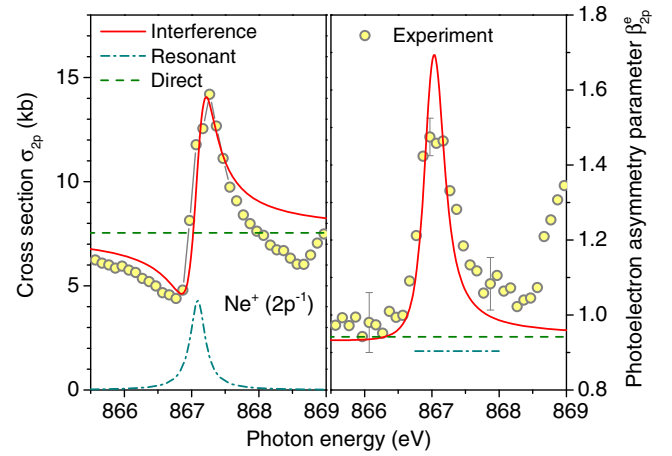


FIG. 2. Photoionization cross section (left panel) and angular distribution parameter (right panel) computed (solid line) and measured (open circles) in the vicinity of the Ne $1s \rightarrow 3p$ excitation for the participator $\text{Ne}^+(2p^{-1})$ final ionic state (unresolved $2p_{1/2,3/2}^{-1}$ doublet). The experimental cross sections is set on the absolute scale with the help of the present theoretical data, whereas no normalization for the asymmetry parameter is required. The individual contributions computed for the direct and resonant ionization channels are also shown by broken curves (see the legend).

spectrum of Ne for process (2). On the high-energy side, experimental $\sigma_{2p}(\omega)$ and $\beta_{2p}^e(\omega)$ exhibit clear signatures of the subsequent $4p$ state. The latter was not included in the present calculations. This explains the slight disagreement between the computed and measured spectra above 868 eV. The individual contribution of the direct (green dashed line) and resonant (cyan dash-dotted curve) ionization channels to $\sigma_{2p}(\omega)$ have similar magnitudes (left panel of Fig. 2). As a consequence, the interference results in the prominent Fano-type profile in the cross section.

The β_{2p}^e computed separately for the direct ionization channel is equal to 0.94 (right panel of Fig. 2). The only experimental off-resonance value known from literature is $\beta_{2p}^e(930 \text{ eV}) = 0.98$ [44]. Both values agree very well with the off-resonance value of 0.98 ± 0.08 measured in the present work on the low-energy side of the $3p$ resonance. The computed resonant value $\beta_{2p}^e = 0.90$ is very close to that of the direct ionization channels. It is in itself a very impressive fact that the counterintuitive interference between these two channels in Ne is also present. A very good agreement between the theory and the experiment seen in Fig. 2 and the similar peak-type dispersion of $\beta_{2p}^e(\omega)$ across the $3p$ resonance in Ne both support reliability of the electronic ionization amplitudes computed in the present work for CH_4 .

We now turn back to methane and discuss the excitation intensity borrowing mechanism by means of vibronic coupling. As discussed in Refs. [15–19], the dipole-forbidden $1s_{a_1} \rightarrow ns_{a_1}$ electronic transitions are vibronically allowed

through the $nsa_1 \leftrightarrow n\ell t_2$ coupling by molecular-field interactions. Exact calculations of the underlying multidimensional nuclear dynamics are extremely complicated [17]. For the present purposes, it is sufficient to model a mechanism in which the nsa_1 Rydberg states borrow excitation intensity from the npt_2 and ndt_2 ones. Strictly, total adiabatic wave functions of excited states are given by combinations of the products of the diabatic electronic and vibrational states [2,5]. By averaging exact solutions over the nuclear coordinates within the Franck-Condon region for excitation, one can approximate adiabatic electronic wave functions of the dipole-forbidden resonances by the following simplified linear combinations: $|NS\rangle = \alpha|nsa_1\rangle + \gamma|npt_2\rangle + \delta|ndt_2\rangle$. The diabatic one-electron wave functions of Rydberg states on the right-hand side of this equation are those listed in Table I. The mixing coefficients α , γ , δ were free parameters in the present simulations, while energy structure of the additionally included vibronic states $\nu_2 - \nu_4$ was taken from Refs. [17–19].

Obviously, the $|NS\rangle$ electronic resonances acquire the excitation probability for any nonzero mixing coefficients γ and δ . This fact is illustrated in the upper panel of Fig. 1 by the red short-dashed curve (VC Excitation). In this simulation, we used the mixing coefficients which were optimized in the final calculation (see below). The simulated cross section $\sigma_X(\omega)$ now exhibits distinct resonant structures around 287.0 eV and between 287.3 and 287.5 eV. These structures are associated with the $3s(\nu_3, \nu_4)$ vibronic states [17–19] (see the assignment at the top of the figure). In addition, the $3p(\nu_2, \nu_4)$ vibronic states were analogously included in this simulation, and they appear in the computed $\sigma_X(\omega)$ between 288.2 and 288.3 eV [17–19] owing to the same mechanism.

Simultaneously, the new resonant structures emerge in the computed $\beta_X^e(\omega)$ parameter (cf. the blue dash-dotted and red short-dashed curves in the lower panel of Fig. 1). Importantly, in the energy range 286.5–288.0 eV, the computed $\beta_X^e(\omega)$ parameter exhibits now a pronounced dip across the $3s(\nu_3, \nu_4)$ resonances, which is in good agreement with the measured $\beta_X^e(\omega)$ dispersion. Unfortunately, structures above the photon energy of 288.0 eV still show the peak-type dispersions of $\beta_X^e(\omega)$ across the $n\ell\nu_1$ and $3p(\nu_2, \nu_4)$ resonances, which is in contradiction to the measured dispersion. Nevertheless, this interesting result gave us an important hint for the solution of the present problem.

We notice that the resonant β_X^e parameter computed for the individual $3s(\nu_3, \nu_4)$ states is equal to zero. The $3s$ Rydberg electron has a rather large partial decay rate for this participator decay channel (the last column in Table I), which dictates this intuitively expected dip in $\beta_X^e(\omega)$ between 286.5 and 288.0 eV. Importantly, the presently computed decay rate Γ_X^{3s} is more than ten times larger than the rates Γ_X^{3p} and Γ_X^{3d} . An interesting question immediately arises. As discussed above, the nsa_1 and $n\ell t_2$ one-electron

wave functions are vibronically coupled by molecular-field interactions. What happens if the $3p$ and $3d$ Rydberg electrons borrow a small part of the partial Auger decay rate from the $3s$ electron? In order to answer this question, we additionally approximated electronic wave functions of the dipole-allowed resonance by the following linear combinations, $|NP\rangle = -\gamma|nsa_1\rangle + \alpha'|npt_2\rangle$ and $|ND\rangle = -\delta|nsa_1\rangle + \alpha''|ndt_2\rangle$, and performed an optimization of the mixing coefficients to obtain the best agreement of the computed and measured dispersions $\beta_X^e(\omega)$.

Results of this final simulation are reflected in Fig. 1 by black solid curves. The following mixing coefficients were used in the calculations: $|\alpha|^2 \approx 89\%$, $|\gamma|^2 \approx 7\%$, and $|\delta|^2 \approx 4\%$ for $|NS\rangle$ vectors; $|\gamma|^2 \approx 7\%$ and $|\alpha'|^2 \approx 93\%$ for $|NP\rangle$ vectors; and $|\delta|^2 \approx 4\%$ and $|\alpha''|^2 \approx 96\%$ for $|ND\rangle$ vectors. From the lower panel of this figure, one can see that even such relatively small admixtures of the $|nsa_1\rangle$ states to the dipole-allowed $|n\ell t_2\rangle$ resonances change the computed $\beta_X^e(\omega)$ dispersions dramatically and establish very good agreement between the present theory and the experiment. Further improvements of the present theory would require full multidimensional calculations of the essentially coupled electron and nuclear dynamics in methane. As a final point, we notice that the proposed decay rate borrowing mechanism enhances the computed partial decay rates Γ_X^{NP} and Γ_X^{ND} (and also the respective branching ratios for this participator decay channel) about twice. As a consequence, the computed cross section significantly grows for the photon energies above 287.5 eV (cf. the red short-dashed and black solid curves in the upper panel of Fig. 1). It now reproduces the presently measured relative intensities of the resonances and the experimental energy dependence $\sigma_X(\omega)$ overall.

In conclusion, we report a joint theoretical and experimental study of the resonant Auger decay of the core-to-Rydberg excited CH_4 and Ne and analyze the angle-resolved participator Auger electron spectra corresponding to the respective ground final ionic states $\text{CH}_4^+(X 1t_2^{-1})$ and $\text{Ne}^+(2p^{-1})$. It is demonstrated that vibronic coupling effects, which are known to facilitate dipole-forbidden transitions in the angle-averaged spectra via the excitation intensity borrowing mechanism, play a decisive role in the formation of the Auger electron angular distributions. Specifically, the presently measured angle-resolved spectra of CH_4 cannot be interpreted theoretically without involving the decay rate borrowing mechanism via vibronic coupling. One may expect a similar effect of vibronic coupling in the final ionic state $\text{CH}_4^+(X 1t_2^{-1})$ on the individual electron angular distributions for the vibrationally resolved manifold of close-lying final vibrational sublevels [13]. The presently uncovered effects are generally expected in polyatomics and solids, which makes angle-resolved Auger spectroscopy a very sensitive tool for accessing information on the vibronic coupling strength, even if it is not accessible in the angle-averaged spectra.

We thank E. Robert for the technical assistance, and the SOLEIL staff for the stable operation of the equipment and the storage ring during the experiments. This work was supported by the State Hessen Initiative for the Development of Scientific and Economic Excellence (LOEWE) within the focus project Electron Dynamics of Chiral Systems (ELCH). Financial support from the Deutsche Forschungsgemeinschaft (DFG Project No. DE 2366/1-1), the Russian Foundation for Basic Research (Grant No. 16-03-00771a), and the Southern Federal University within Inner Project No. 213.01.-07.2014/11PPIG is gratefully acknowledged. I. D. P. would like to thank the Institute of Physics, University of Kassel and Ph. V. D. the Research Institute of Physics, Southern Federal University for the hospitality during their respective research stays.

*knie@physik.uni-kassel.de

†Present address: Department of Physics, University of Oulu, P.O. Box 3000, 90014 Oulu, Finland.

‡demekhin@physik.uni-kassel.de

- [1] T. Azumai and K. Atsuzaki, *Photochem. Photobiol.* **25**, 315 (1977).
- [2] H. Köppel, W. Domcke, and L. S. Cederbaum, *Adv. Chem. Phys.* **57**, 59 (1984).
- [3] G. Fischer, *Vibronic Coupling* (Academic Press, London, 1984).
- [4] G. A. Worth and L. S. Cederbaum, *Annu. Rev. Phys. Chem.* **55**, 127 (2004).
- [5] *Conical Intersections*, edited by W. Domcke, D. R. Yarkony, and H. Köppel (World Scientific, Singapore, 2004).
- [6] M. Baer, *Beyond Born-Oppenheimer: Electronic Non-adiabatic Coupling Terms and Conical Intersections* (Wiley Interscience, Hoboken, NJ, 2006).
- [7] *Multidimensional Quantum Dynamics: MCTDH Theory and Applications*, edited by H.-D. Meyer, F. Gatti, and G. A. Worth (Wiley-VCH, Weinheim, 2009).
- [8] W. Domcke and D. R. Yarkony, *Annu. Rev. Phys. Chem.* **63**, 325 (2012).
- [9] G. Davies, *Rep. Prog. Phys.* **44**, 787 (1981).
- [10] Y. Ma, P. Skytt, N. Wassdahl, P. Glans, D. C. Mancini, J. Guo, and J. Nordgren, *Phys. Rev. Lett.* **71**, 3725 (1993).
- [11] F. Bernardi, M. A. Robb, and M. Olivucci, *Chem. Soc. Rev.* **25**, 321 (1996).
- [12] B. G. Levine and T. J. Martinez, *Annu. Rev. Phys. Chem.* **58**, 613 (2007).
- [13] W. Domcke, *Phys. Scr.* **19**, 11 (1979).
- [14] Th. Zimmermann, H. Köppel, and L. S. Cederbaum, *J. Chem. Phys.* **91**, 3934 (1989).
- [15] P. Bagus, M. Krauss, and R. E. LaVilla, *Chem. Phys. Lett.* **23**, 13 (1973).
- [16] A. P. Hitchcock, M. Pocock, and C. E. Brion, *Chem. Phys. Lett.* **49**, 125 (1977).
- [17] J. Schirmer, A. B. Trofimov, K. J. Randall, J. Feldhaus, A. M. Bradshaw, Y. Ma, C. T. Chen, and F. Sette, *Phys. Rev. A* **47**, 1136 (1993).
- [18] G. Remmers, M. Domke, and G. Kaindl, *Phys. Rev. A* **47**, 3085 (1993).
- [19] K. Ueda, M. Okunishi, H. Chiba, Y. Shimizu, K. Ohmori, Y. Sato, E. Shigemasa, and N. Kosugi, *Chem. Phys. Lett.* **236**, 311 (1995).
- [20] V. Schmidt, *Rep. Prog. Phys.* **55**, 1483 (1992).
- [21] Ph. V. Demekhin, I. D. Petrov, V. L. Sukhorukov, W. Kielich, P. Reiss, R. Hentges, I. Haar, H. Schmoranzer, and A. Ehresmann, *Phys. Rev. A* **80**, 063425 (2009); **81**, 069902(E) (2010).
- [22] Ph. V. Demekhin, I. D. Petrov, T. Tanaka, M. Hoshino, H. Tanaka, K. Ueda, W. Kielich, and A. Ehresmann, *J. Phys. B* **43**, 065102 (2010).
- [23] C. Miron, V. Kimberg, P. Morin, C. Nicolas, N. Kosugi, S. Gavriluyuk, and F. Gel'mukhanov, *Phys. Rev. Lett.* **105**, 093002 (2010).
- [24] Ph. V. Demekhin, I. D. Petrov, V. L. Sukhorukov, W. Kielich, A. Knie, H. Schmoranzer, and A. Ehresmann, *Phys. Rev. Lett.* **104**, 243001 (2010).
- [25] Ph. V. Demekhin, I. D. Petrov, V. L. Sukhorukov, W. Kielich, A. Knie, H. Schmoranzer, and A. Ehresmann, *J. Phys. B* **43**, 165103 (2010).
- [26] A. Lindblad, V. Kimberg, J. Söderström, C. Nicolas, O. Travnikova, N. Kosugi, F. Gel'mukhanov, and C. Miron, *New J. Phys.* **14**, 113018 (2012).
- [27] C. Miron and P. Morin, in *Handbook of High-resolution Spectroscopy*, edited by M. Quack and F. Merkt (John Wiley & Sons, Chichester, England, 2011).
- [28] Y.-K. Kim, W. Hwang, N. M. Weinberger, M. A. Ali, and M. E. Rudd, *J. Chem. Phys.* **106**, 1026 (1997).
- [29] B. M. Lagutin, I. D. Petrov, V. L. Sukhorukov, S. Kammer, S. Mickat, R. Schill, K.-H. Schartner, A. Ehresmann, Yu. A. Shutov, and H. Schmoranzer, *Phys. Rev. Lett.* **90**, 073001 (2003).
- [30] B. M. Lagutin, I. D. Petrov, V. L. Sukhorukov, Ph. V. Demekhin, B. Zimmermann, S. Mickat, S. Kammer, K.-H. Schartner, A. Ehresmann, Y. A. Shutov, and H. Schmoranzer, *J. Phys. B* **36**, 3251 (2003).
- [31] G. S. Brown, M. H. Chen, B. Crasemann, and G. E. Ice, *Phys. Rev. Lett.* **45**, 1937 (1980).
- [32] A. Kivimäki, A. Naves de Brito, S. Aksela, H. Aksela, O.-P. Sairanen, A. Ausmees, S. J. Osborne, L. B. Dantas, and S. Svensson, *Phys. Rev. Lett.* **71**, 4307 (1993).
- [33] O. Travnikova, J. C. Liu, A. Lindblad, C. Nicolas, J. Söderström, V. Kimberg, F. Gel'mukhanov, and C. Miron, *Phys. Rev. Lett.* **105**, 233001 (2010).
- [34] J. Söderström, A. Lindblad, A. Grum-Grzhimailo, O. Travnikova, N. Nicolas, S. Svensson, and C. Miron, *New J. Phys.* **13**, 073014 (2011).
- [35] C. Miron, C. Nicolas, O. Travnikova, P. Morin, Y. Sun, F. Gel'mukhanov, N. Kosugi, and V. Kimberg, *Nat. Phys.* **8**, 135 (2012).
- [36] T. X. Carroll, N. Berrah, J. Bozek, J. Hahne, E. Kukk, L. J. Sæthre, and T. D. Thomas, *Phys. Rev. A* **59**, 3386 (1999).
- [37] M. Coreno, L. Avaldi, R. Camilloni, K. C. Prince, M. de Simone, J. Karvonen, R. Colle, and S. Simonucci, *Phys. Rev. A* **59**, 2494 (1999).
- [38] A. Knie, M. Ilchen, Ph. Schmidt, Ph. Reiß, C. Ozga, B. Kambs, A. Hans, N. Mueglichs, S. A. Galitskiy, L. Glaser, P. Walter, J. Viefhaus, A. Ehresmann, and Ph. V. Demekhin, *Phys. Rev. A* **90**, 013416 (2014).

- [39] Ph. V. Demekhin, V. L. Sukhorukov, and A. Ehresmann, *J. Chem. Phys.* **134**, 024113 (2011).
- [40] S. A. Galitskiy, A. N. Artemyev, K. Jänkälä, B. M. Lagutin, and Ph. V. Demekhin, *J. Chem. Phys.* **142**, 034306 (2015).
- [41] F. K. Gel'mukhanov, L. N. Mazalov, and A. V. Kondratenko, *Chem. Phys. Lett.* **46**, 133 (1977).
- [42] A. Cesar and H. Ågren, *Phys. Rev. A* **45**, 2833 (1992).
- [43] A. Kivimäki, M. Neeb, B. Kempgens, H. M. Köppe, and A. M. Bradshaw, *J. Phys. B* **29**, 2701 (1996).
- [44] U. Becker and D. Shirley, in *VUV and Soft X-Ray Photoionization*, edited by U. Becker and D. Shirley (Plenum Press, New York, 1996), p. 135.